Geosci. Model Dev. Discuss., 5, 515–548, 2012
www.geosci-model-dev-discuss.net/5/515/2012/
doi:10.5194/gmdd-5-515-2012

Geoscientific
Model Development
Discussions

Modelling the mid-Pliocene Warm Period climate with the IPSL coupled model and its atmospheric component LMDZ4

C. Contoux[1], G. Ramstein[1], and A. Jost[2,3]

[1]Laboratoire des Sciences du Climat et de l'Environnement/IPSL, CEA-CNRS-UVSQ, UMR8212, Orme des Merisiers, CE Saclay, 91191 Gif-sur-Yvette Cedex, France
[2]UPMC Université Paris 06, UMR7619, Sisyphe, 75005, Paris, France
[3]CNRS, UMR7619, Sisyphe, 75005, Paris, France

Received: 31 January 2012 – Accepted: 10 February 2012 – Published: 17 February 2012

Correspondence to: C. Contoux (camille.contoux@lsce.ipsl.fr)

Published by Copernicus Publications on behalf of the European Geosciences Union.

Abstract

This paper describes the experimental design and model results of the climate simulations of the mid-Pliocene Warm Period (mPWP, ca. 3.3–3 Ma) using the Institut Pierre Simon Laplace model (IPSLCM5A), in the framework of the Pliocene Model Intercomparison Project (PlioMIP). We use the IPSL atmosphere ocean general circulation model (AOGCM), and its atmospheric component alone, to simulate the climate of the mPWP. Boundary conditions such as sea surface temperatures (SSTs), topography, ice sheet extent and vegetation are derived from the ones imposed by the Pliocene Model Intercomparison Project (PlioMIP), described in Haywood et al. (2010, 2011). We first describe the IPSL model main features, and then give a full description of the boundary conditions used for atmospheric model and coupled model experiments. The climatic outputs of the mPWP simulations are detailed and compared to the corresponding control simulations. The simulated warming is 1.94 °C in the atmospheric and 1.83 °C in the coupled model experiments. In both experiments, warming is more important at high latitudes. Simulated precipitation has a different behaviour in the coupled model than in the atmospheric model alone, because of the reduced gradients in imposed SSTs, which impacts the Hadley and Walker circulations. In addition, a sensitivity test to the change of land-sea mask in the atmospheric model, representing a sea-level change from present-day to 25 m higher during the mid-Pliocene, is described. We find that surface temperature differences can be important (several degrees Celsius) but are restricted to the areas that were changed from ocean to land or vice versa. In terms of precipitation, there is no impact on polar regions although the change in land-sea mask is important in these areas.

1 Introduction

The mid-Pliocene Warm Period (mPWP, ca. 3.3–3 Ma) is the most recent period in geological history when Earth experienced a warmer climate than the preindustrial during a sustained period of time, longer than interglacial periods of the last million years. Moreover, the mPWP being a quite recent period at the geological scale, continents position is similar to the present one, and the CO_2 content is very close to present-day one (405 ppm), both conditions making the mPWP a relevant analogue for future global warming. Nevertheless, it must be kept in mind that the mPWP climate is simulated in equilibrium with prescribed boundary conditions whereas the future climate will be very far from equilibrium due to a rapid increase of forcings (Crowley, 1991). One issue is to assess whether or not climate models are able to reproduce a warmer than today climate, and to determine model biases (Crowley, 1996; Salzmann et al., 2009). Availability of data generally decreases when one goes back in time, but the mPWP being a quite recent period and also a sustained one (∼300 000 yr), numerous terrestrial and marine records are available, and made it possible to build datasets that are used for deriving vegetation and sea-surface temperatures (SSTs). These databases include a large quantity of data and allow a more accurate interpretation of the mPWP climate. They are now at a global level that enables comparison with model results. On their side modellers are more and more interested in simulating the mPWP. After the pioneering simulations performed by Chandler et al. (1994); Sloan et al. (1996) and Haywood et al. (2000), it is now a large group who shares similar boundary conditions thanks to the PlioMIP initiative, in order to compare model results. This aspect makes it important to document each group's implementation of boundary conditions, models and their basic results.

2 Model description

The coupled atmosphere-ocean general circulation model (AOGCM) used in this study is IPSLCM5A, which is a higher resolution version of the IPSLCM4 coupled atmosphere-ocean GCM (Marti et al., 2010) that was previously used for CMIP3/IPCC AR4 (Dufresne et al., 2005). A detailed description of the different components can be found in Dufresne et al. (2012). The different components of the model i.e. atmosphere, land surface, ocean and sea-ice are also shortly detailed in the following. All these components are coupled together via the OASIS coupler.

2.1 LMDZ4 atmosphere model

The following description of the LMDZ model is based on Hourdin et al. (2006) and Hourdin et al. (2012). Details about the physical parametrisation can be found in Hourdin et al. (2006). LMDZ is the climate model developed at Laboratoire de Météorologie Dynamique, in Paris. This model has the specificity to be zoomed (the Z of LMDZ) if necessary on a specific region and then may be used for regional studies (e.g., Jost et al., 2009). Atmosphere dynamics is represented by a finite-difference discretisation of the primitive equations of meteorology (e.g., Sadourny and Laval, 1984) on a longitude-latitude Arakawa C-grid (e.g., Kasahara, 1977). The chosen resolution of the model is 96 × 95 × 39, corresponding to an interval of 3.75 degrees in longitude and 1.9 degrees in latitude. Resolution was improved from 19 to 39 vertical levels, with around 15 levels above 20 km, its resolution in the stratosphere being close to a previous stratospheric version of LMDZ4 described by Lott et al. (2005). A leapfrog scheme is used for time integration. The Morcrette (1991) scheme is used for radiative transfer. Effects of the subgrid scale orography are parametrised according to Lott (1999).

2.2 ORCHIDEE land surface model

ORCHIDEE (Organizing Carbon and Hydrology In Dynamic Ecosystems, Krinner et al., 2005) is composed of three modules: hydrology, carbon cycle and vegetation dynamics. The hydrological module, SECHIBA (Ducoudré et al., 1993; de Rosnay and Polcher, 1998), describes exchange of energy and water between atmosphere and biosphere, and the soil water budget (Krinner et al., 2005). The river routing scheme combines the river flow with a cascade of three reservoirs: the stream and two soil reservoirs with different time constants (Marti et al., 2010). Vegetation dynamics parametrisation is derived from the dynamic global vegetation model LPJ (Sitch et al., 2003; Krinner et al., 2005). The carbon cycle model simulates phenology and carbon dynamics of the terrestrial biosphere (Krinner et al., 2005). Vegetation distributions are described using 13 plant functional types (PFTs) including agricultural C3 and C4 plants, which are not used in the mPWP simulations, bringing down the number of PFTs to 11, including bare soil. The description of land ice included in ORCHIDEE is not used when coupled to the atmosphere (Marti et al., 2010), land ice being treated by LMDZ in this case. In our case, hydrology and carbon modules are activated, but vegetation is prescribed using 11 PFTs, derived from the PRISM Biomes dataset (Salzmann et al., 2008). Therefore, soil, litter, and vegetation carbon pools (including leaf mass and thus LAI) are calculated as a function of dynamic carbon allocation (Krinner et al., 2005).

2.3 NEMO ocean model

The ocean model version is NEMOv3.2 (Nucleus for European Modelling of the Ocean, Madec, 2008), used with a resolution of 182 × 149 × 31. We summarize here the main characteristics of the model as described by Marti et al. (2010). Details of the ocean physics and boundary conditions can be found in Madec et al. (1997). The ocean configuration ORCA2.3 uses a tripolar grid with horizontal curvilinear mesh (Madec and Imbard, 1996; Murray, 1996), with two poles in the Northern hemisphere, over Canada and Siberia, to overcome the North Pole singularity. Mean grid spacing is about 2/3°. Latitudinal resolution is refined to 1 degree near the equator and in the Mediterranean Sea. The Gibraltar Strait has a width of 111 km, and is explicitly resolved. There are 31 vertical levels in the ocean, with 10 levels in the top 100 m. A total variance dissipation scheme is used for advection of temperature and salinity (Lévy et al., 2001; Cravatte et al., 2007). A conservation scheme of both energy and enstrophy is used in the momentum equation (Arakawa and Lamb, 1981; Le Sommer et al., 2009).

2.4 LIM sea-ice model

The sea-ice model used is LIM2 (Louvain-la-Neuve Sea Ice Model), a thermodynamic-dynamic sea ice model described in Fichefet and Morales-Maqueda, 1997, 1999. We present here the main features of the model as described in the latter paper (Fichefet and Morales-Maqueda, 1999). A three-layer model determines vertical heat conduction and sensible heat storage inside ice and snow. There is one layer for snow and two layers for ice. Trapping of shortwave radiation by brine pockets resulting in latent heat storage inside the ice is taken into account. The model also allows for the presence of leads within the ice pack. Vertical and lateral growth/decay rates are obtained from the prognostic energy budgets at both the bottom and surface boundaries of the snow-ice cover and in leads. Surface albedo is parametrised as a function of surface temperature and of snow and ice thicknesses. LIM runs on the same grid than NEMO (Marti et al., 2010).

3 Experimental design

3.1 Pre-industrial

For the AGCM experiments, the Control simulation boundary conditions (i.e. SSTs, vegetation, topography and ice sheet extents) are set to modern. Imposed SSTs are the mean value for 1988–2007. Greenhouse gases, solar constant and orbital parameters are set to Pre-industrial values as required by CMIP5/PMIP3, i.e. solar constant is 1365 $\mathrm{W\,m^{-2}}$, CO_2 content is 280 ppm, CH_4 content is 760 ppb, and N_2O content is 270 ppb. For the AOGCM experiments, the Control simulation was performed as required by CMIP5/PMIP3 by the LSCE modelling group. It is a 2800 yr simulation which already started from equilibrium conditions.

3.2 Mid-Pliocene

The experimental design and boundary conditions follow the protocol of “alternate” simulations described in Haywood et al. (2010) for AGCM and AOGCM simulations. Boundary conditions are built on a modern coastline, because of the challenge of changing the land-sea mask in the ocean model. Since a modern coastline makes the simulation a little unrealistic to be able to compare with data (especially on coastal areas), we decided to perform an AGCM simulation with “preferred” boundary conditions, named Plio1_pref. The difference between results from “alternate” and “preferred” AGCM simulations will be discussed in Sect. 4.4. The AGCM outputs presented below are the ones with alternate boundary conditions, named Plio1_alt.

3.2.1 Boundary conditions

For experiment 1 (i.e. for AGCM simulation, as defined in Haywood et al., 2010), two simulations were performed: the first with modern land-sea mask, called Plio1_alt, and the second with Pliocene land-sea mask, Plio1_pref, corresponding to a 25-m sea level rise (Fig. 1). The boundary conditions implemented were these given in Haywood et al. (2010), “alternate” set of boundary conditions for Plio1_alt, and “preferred” set for Plio1_pref. Both experiments use the anomaly method for implementation of topography and SSTs. For topography, the difference between the mid-Pliocene topographic reconstruction (Sohl et al., 2009) and the modern topography provided by the PRISM group (Edwards et al., 1992) was added to the IPSL model topography (Fig. 2). When the resulting topography was lower than zero, absolute mid-Pliocene topography was implemented. The same method was used for SSTs, the difference between the mid-Pliocene SST reconstruction (Dowsett, 2007b; Robinson et al., 2008; Dowsett and Robinson, 2009; Dowsett et al., 2009) and the modern SSTs provided by the PRISM group (Reynolds and Smith, 1995) was added to the IPSL model SSTs (Fig. 3). The ice sheet extent is changed to mid-Pliocene conditions using the PRISM3 ice-sheet reconstruction (Hill et al., 2007; Salzmann et al., 2008; Hill, 2009). For the change of vegetation, the BIOME4 dataset provided by the PRISM3 project (Salzmann et al., 2008) was converted into 11 plant functional types (PFTs) (Table 1 and Fig. 4) to be used as boundary conditions in the IPSL model. Ocean gateways were not changed compared to preindustrial conditions (Fig. 1). For river routing and soils, no modification was done. For experiment 2 (i.e. with the AOGCM), the outputs of the "alternate" AGCM simulation are used as a forcing for atmosphere, land surface and carbon cycle components. The ocean starts from the CMIP5/PMIP3 control experiment outputs. For each mid-Pliocene simulation, solar constant, greenhouse gases, aerosols and orbital parameters are the same than in the Control run except for CO_2 that was prescribed to 405 ppm as required by Haywood et al. (2010).

3.2.2 Spin-up and climatological means

For AGCM experiments (Control, Plio1_alt and Plio1_pref) the spin up was set to 20 yr and presented results are 30 yr-climatological-means, as required by Haywood et al. (2010). For AOGCM experiment, the spin-up was set to 350 yr and the integration length is set to 50 yr, since the simulation only achieved 400 yr up to now (Fig. 5).

4 Results

4.1 Surface temperature

Mean annual global values for the main variables can be found in Table 2. With the AGCM, mean annual global warming is 1.94 °C compared to the control simulation. The mid-Pliocene mean annual temperature is 17 °C, which is similar to the value obtained with MIROC AGCM (16.68 °C, Chan et al., 2011). Warming is more important at high latitudes with an anomaly of +10 °C at 80° N, and +7.5 °C at 70° S (Figs. 6 and 7). With the coupled AOGCM, a similar warming of +1.83 °C is found, although warming at high latitudes is less important, particularly for the Northern part, where warming at

80° N only reaches +4 °C (Figs. 6 and 8). In the AGCM simulation results, patterns of several degrees of cooling also appear, particularly in June-July-August for regions of the Northern hemisphere, namely Central and Eastern Africa, India and the Himalaya; and in December-January-February over Australia (Fig. 7). These cooling patterns do not exist in the AOGCM simulation, which on the opposite, shows a small warming in these regions (Fig. 8). These differences can be explained by the difference between calculated SSTs and imposed SSTs (Fig. 11). Changes of temperature on mountain regions, that are similar in both simulations, can be explained by the change in topography. Regions which show a cooling coincide with higher elevation during the mid-Pliocene: Eastern Antarctica, eastern part of the Andes, eastern part of the Rocky Mountains, southern Himalaya. Conversely, increase in temperature is found where topography is lower: coastal Eastern Antarctica, West Antarctica, Western Greenland, Western Andes, Western Rocky mountains and Northern Himalayas. On Greenland and Antarctica, the removal of the ice sheets creates an important warming which is due to both albedo and topography effects. Simulated warming over Greenland and Antarctica is similar in the AGCM and AOGCM, with temperature anomalies reaching +25 to +30 °C. These values are similar to the AGCM results of Koenig et al. (2012). In the tropics, warming is more important in the AOGCM simulation than in the AGCM simulation (Fig. 6).

4.2 Precipitation

Although there is almost no change in the global values of precipitation, (Table 2, +0.05 mm day^{-1} for AGCM, and +0.11 mm day^{-1} for AOGCM), precipitation patterns are significantly impacted in the AGCM (Fig. 10, upper panel). Indeed, there are important changes at low latitudes: precipitation increases in many regions like Central Africa, Northern and Eastern Australia, and some parts of the Amazon Basin. Meanwhile, precipitation decreases in the tropical Indian and Pacific Oceans. These differences are similar to those observed with the MRI-AGCM, explained by a general slowing down of the Walker circulation due to the reduced East-West SST gradient in the tropics, (Kamae et al., 2011), which induces a broadening of the ITCZ (Figs. 9 and 10, AGCM). There is also an increase in precipitation over the North Atlantic region, where imposed SSTs show an important warming (Fig. 10, AGCM). Previous studies using PRISM2 boundary conditions (Dowsett et al., 1999; Dowsett, 2007a) and AGCM (Haywood et al., 2009) have shown that the large changes in high latitude SSTs versus mostly unchanged equatorial SSTs produce a large weakening of the Hadley cell. This feature is indeed amplified by albedo feedback due to the reduction of sea ice and land ice cover (Koenig et al., 2012). The same mechanism is observed but for cold conditions when an AGCM simulates the Last Glacial Maximum climate: due to the increase of the equator to pole gradient, the Hadley cell increases (Ramstein et al., 1998; Jost et al., 2005). More recently, using the new dataset PRISM3 (Dowsett, 2007b; Robinson et al., 2008; Dowsett and Robinson, 2009; Dowsett et al., 2009), new AGCM simulations also depict that the large scale pattern of mid-Pliocene SSTs induces a major re-organisation of atmospheric circulation. First the Hadley cell response is shown to weaken with its ascending branches extending polewards (Kamae et al., 2011; Yan et al., 2011). Moreover the data provided over Pacific with a western tropical Pacific unchanged but an Eastern Pacific temperature increase of around 4 °C induce a weakening of the Walker cell which has been interpreted as a permanent El-Niño (Ravelo et al., 2004). This pattern has been shown to explain large scale precipitation changes (Kamae et al., 2011). All these features are also observed in our simulation, especially concerning the precipitation pattern. This is the response of AGCM to SST changes. Most of PlioMIP AGCMs may depict these important features. However, in the AOGCM, precipitation response is different from the AGCM one. There is no important change in the precipitation pattern, and precipitation in the ITCZ increases. These differences between AGCM and AOGCM are explained by the differences between calculated SSTs in the AOGCM and imposed SSTs in the AGCM (Fig. 11).

4.3 Sea surface temperature

One of the challenges of coupled model simulations is to investigate if the North Atlantic high warming pattern inferred from SST reconstructions can be reproduced. Available simulations with AOGCM reproduce some warming in the Greenland Sea (Fig. 12 and also Zhang et al., 2012) but are unsuccessful in reproducing the global warming pattern occurring in the whole Greenland and Norwegian Seas, and in North Atlantic (Fig. 11 and also Chan et al., 2011; Zhang et al., 2012). In detail, warmer SSTs in our simulation occur in the Greenland and Northern Norwegian Seas (Fig. 12) whereas in Zhang et al. (2012), warmer SSTs occur in the Greenland Sea, but also in the Central North Atlantic. These differences between two AOGCMs are a very interesting feature to help us understand which processes and which feedbacks permit to sustain high temperatures over North Atlantic and the Nordic Seas. On the other hand we have to keep a critical eye on alkenone data, which could possibly represent summer temperatures (Leduc et al., 2010). The other main interest of coupled AOGCM simulations is to investigate whether the East-West SST gradient is reduced in the tropical Pacific. In our simulation, the Pacific warms uniformly (Fig. 12), there is no differential warming in the Eastern Pacific which could induce a reduction of the East-West gradient. This reconstructed pattern of warming in the Eastern tropical Pacific could be related with variability in the Pacific, which may not be properly captured by AOGCM simulations (Ravelo et al., 2004).

4.4 Sensitivity test to the change of land-sea mask in the AGCM

The surface temperature and total precipitation differences between the AGCM simulation with “preferred” boundary conditions and the one with “alternate” boundary conditions can be seen on Fig. 13. Significant changes of surface temperature appear where grid cells were turned from land to sea, or conversely. The largest warming signal is observed on the Hudson Bay and on the coast of Eastern Antarctic. However, this temperature change is not correlated with a precipitation change. It seems that turning land to ocean around West-Antarctic ice sheet does not directly impact the hydrological cycle.

5 Summary and conclusions

The mid-Pliocene Warm Period is the last sustained period of time (3.3 to 3 Ma) when temperatures reached 2 to 3 °C of warming compared to today. Sea surface temperature reconstructions show that warming is more important at high latitudes, and so does model results. Since the mid-Pliocene Warm Period can be considered as an interesting period to compare with future global warming in terms of CO_2 concentration and magnitude of the warming, this period is of high interest for understanding feedbacks and mechanisms that sustained such a warm climate. The PlioMIP will help understand the strengths and weaknesses of each model when simulating a warmer than today climate. Areas where there is a model/data mismatch may be good targets to understand regional features. Multi-model comparison can also help us to pinpoint the processes involved in such a warming. In this study, we described the implementation of the PRISM boundary conditions in our model, which closely followed the guidelines of PlioMIP (Haywood et al., 2010, 2011). The main difference with the guidelines is that we started the ocean model from pre-industrial control conditions, and did not include any mid-Pliocene ocean temperatures reconstructions to force the ocean model. We implemented the "alternate" set of boundary conditions for simulations with AGCM and AOGCM, and included the results of one additional experiment with the AGCM, this time with "preferred" boundary conditions. This sensitivity test showed to have an important impact on coastal surface temperature, but a weak impact on precipitation especially over the polar regions. For mid-Pliocene AGCM simulation, we find a global warming of 1.94 °C, which is in agreement with previous simulations with AGCMs (Koenig et al., 2012; Yan et al., 2011), and a broadening of the ITCZ due to reduced SST gradients, also in good agreement with other AGCM results (Kamae et al., 2011; Yan et al., 2011). For the AOGCM simulation, the global simulated warming is 1.83 °C, a value close to the one observed by Zhang et al., (+2 °C, 2012). We find that precipitation patterns are different in AGCM and AOGCM, due to the inability of the AOGCM to reproduce SST reconstructed patterns. To conclude, it is now important to focus on the multi-model analysis, to determine which processes are well reproduced and what are the governing mechanisms under a warmer climate.

Acknowledgements. We thank Pierre Sepulchre and Masa Kageyama for their help with the model and Arnaud Caubel for providing Pre-industrial control simulations with the coupled model. Many thanks to Jean-Yves Peterschmitt for technical assistance.

cnrs INSU
Institut national des **sciences** de **l'Univers**

The publication of this article is financed by CNRS-INSU.

References

Arakawa, A. and Lamb, V. R.: A potential enstrophy and energy conserving scheme for the shallow water equations, Mon. Weather Rev., 109, 18–36, 1981. 519

Chan, W.-L., Abe-Ouchi, A., and Ohgaito, R.: Simulating the mid-Pliocene climate with the MIROC general circulation model: experimental design and initial results, Geosci. Model Dev., 4, 1035–1049, doi:10.5194/gmd-4-1035-2011, 2011. 522, 525

Chandler, M. A., Rind, D., and Thompson, R. S.: Joint investigations of the middle Pliocene climate II: GISS GCM Northern Hemisphere results, Global Planet. Change, 9, 197–219, 1994. 517

Cravatte, S., Madec, G., Izumo, T., Menkes, C., and Bozec A.: Progress in the 3-D circulation of the eastern equatorial Pacific in a climate ocean model, Ocean Model., 17, 28–48, doi:10.1016/j.ocemod.2006.11.003, 2007. 519

Crowley, T. J.: Modeling Pliocene warmth, Quat. Sci. Rev., 10, 272–282, 1991. 517

Crowley, T. J.: Pliocene climates: The nature of the problem, Mar. Micropaleontol., 27, 3–12, 1996. 517

de Rosnay, P. and Polcher, J.: Modelling root water uptake in a complex land surface scheme coupled to a GCM, Hydrol. Earth Syst. Sci., 2, 239–255, doi:10.5194/hess-2-239-1998, 1998. 518

Dowsett, H. J.: The PRISM Palaeoclimate Reconstruction and Pliocene Sea-Surface Temperature, in: Deep Time Perspectives on Climate Change: Marrying the Signal from Computer Models and Biological Proxies, edited by: Williams, M., Haywood, A. M., Gregory, F. J., and Schmidt, D. H., Micropalaeontol. Soc., Spec. Pub. Geol. Soc., London, 517–538, 2007a. 524

Dowsett, H. J.: Faunal re-evaluation of Mid-Pliocene conditions in the western equatorial Pacific, Micropaleontology, 53, 447–456, 2007b. 521, 524

Dowsett, H. J. and Robinson, M. M.: Mid-Pliocene equatorial Pacific sea surface temperature reconstruction: a multi-proxy perspective, Phil. Trans. R. Soc. A, 367, 109–126, 2009. 521, 524

Dowsett, H. J., Barron, J. A., Poore, R. Z., Thompson, R. S., Cronin, T. M., Ishman, S. E., and Willard, D. A.: Pliocene Paleoenvironmental Reconstruction, US Geological Survey Open File Report, 99–535, 1999. 524

Dowsett, H. J., Robinson, M. M., and Foley, K. M.: Pliocene three-dimensional global ocean temperature reconstruction, Clim. Past, 5, 769–783, doi:10.5194/cp-5-769-2009, 2009. 521, 524

Ducoudré, N. I., Laval, K., and Perrier, A.: SECHIBA, a new set of parameterizations of the hydrologic exchanges at the land-atmosphere interface within the LMD atmospheric general circulation model, J. Climate, 6, 248–273, 1993. 518

Dufresne, J.-L., Quaas, J., Boucher, O., Denvil, S., and Fairhead, L. Contrasts in the effects on climate of anthropogenic sulfate aerosols between the 20th and the 21st century, Geophys. Res. Lett., 32, L21703, doi:10.1029/2005GL023619, 2005. 517

Dufresne, J.-L., Foujols, M-A., Denvil, S., Caubel, A., Marti, O., Aumont, O., Balkanski, Y., Bekki, S., Bellenger, H., Benshila, R., Bony, S., Bopp, L., Braconnot, P., Brockmann, P., Cadule, P., Cheruy, F., Codron, F., Cozic, A., Cugnet, D., de Noblet, N., Duvel, J.-P., Ethé, C., Fairhead, L., Fichefet, T., Flavoni, S., Friedlingstein, P., Grandpeix, J.-Y., Guez, L., Guilyardi, E., Hauglustaine, D., Hourdin, F., Idelkadi, A., Ghattas, J., Joussaume, S., Kageyama, M., Krinner, G., Labetoulle, S., Lahellec, A., Lefebvre, M.-P., Lefevre, F., Levy, C., Li, Z.-X., Lloyd, J., Lott, F., Madec, G., Mancip, M., Marchand, M., Masson, S., Meurdesoif, Y., Mignot, J., Musat, I., Parouty, S., Polcher, J., Rio, C., Schulz, M., Swingedouw, D., Szopa, S., Talandier, C., Terray, P., and Viovy, N.: Climate change projections using the IPSL-CM5 Earth System Model: from CMIP3 to CMIP5, submitted, Clim. Dynam., 2012. 517

Edwards, M.: Global Gridded Elevation and Bathymetry. In: Global Ecosystems Database, Version 1.0 (on CD-ROM), Documentation Manual, Disc-A: National Geophysical Data Center, Key to Geophysical Records Documentation No. 26, Incorporated in: Global Change Database, Vol. 1, edited by: Kineman, J. J. and Ohrenschall, M. A., Boulder, CO, National Oceanic and Atmospheric Administration, A14-1–A14-4, 1992. 521

Fichefet, T. and Morales-Maqueda, M. A.: Sensitivity of a global sea ice model to the treatment of ice thermodynamics and dynamics, J. Geophys. Res., 102, 12609–12646, doi:10.1029/97JC00480, 1997. 520

Fichefet, T. and Morales-Maqueda, M. A.: Modelling the influence of snow accumulation and snow-ice formation on the seasonal cycle of the Antarctic sea-ice cover, Clim. Dynam., 15, 251–268, doi:10.1007/s003820050280, 1999. 520

Haywood, A. M., Valdes, P. J., and Sellwood, B. W.: Global scale palaeoclimate reconstruction of the middle Pliocene climate using the UKMO GCM: initial results, Global Planet. Change, 25, 239–256, 2000. 517

Haywood, A. M., Chandler, M. A., Valdes, P. J., and Salzmann, U.: Comparison of mid-Pliocene climate predictions produced by the HadAM3 and GCMAM3 General Circulation Models, Global Planet. Change, 66, 208–224, 2009. 524

Haywood, A. M., Dowsett, H. J., Otto-Bliesner, B., Chandler, M. A., Dolan, A. M., Hill, D. J., Lunt, D. J., Robinson, M. M., Rosenbloom, N., Salzmann, U., and Sohl, L. E.: Pliocene Model Intercomparison Project (PlioMIP): experimental design and boundary conditions (Experiment 1), Geosci. Model Dev., 3, 227–242, doi:10.5194/gmd-3-227-2010, 2010. 516, 521, 522, 526

Haywood, A. M., Dowsett, H. J., Robinson, M. M., Stoll, D. K., Dolan, A. M., Lunt, D. J., Otto-Bliesner, B., and Chandler, M. A.: Pliocene Model Intercomparison Project (PlioMIP): experimental design and boundary conditions (Experiment 2), Geosci. Model Dev., 4, 571–577, doi:10.5194/gmd-4-571-2011, 2011. 516, 526

Hill, D. J.: Modelling Earth's Cryosphere during Pliocene Warm Peak, Ph.D. thesis, University of Bristol, UK, 368 pp., 2009. 521

Hill, D. J., Haywood, A. M., Hindmarsh, R. C. A., and Valdes, P. J. Characterising ice sheets during the mid-Pliocene: evidence from data and models, In: Deep Time Perspectives on

Climate Change: Marrying the Signal from Computer Models and Biological Proxies, edited by: Williams, M., Haywood, A. M., Gregory, F. J., and Schmidt, D. H., Micropalaeontol. Soc., Spec. Pub. Geol. Soc., London, 517–538, 2007. 521

Hourdin, F., Musat, I., Bony, S., Braconnot, P., Codron, F., Dufresne, J.-F., Fairhead, L., Filiberti, M.-A., Friedlingstein, P., Grandpeix, J.-Y., Levan, P., Li, Z.-X., and Lott, F.: The LMDZ4 general circulation model: climate performance and sensitivity to parametrized physics with emphasis on tropical convection, Clim. Dynam., 27, 787–813, 2006. 518

Hourdin F., Foujols, M.-A., Codron, F., Guemas, V., Dufresne, J.-L., Bony, S., Denvil, S., Guez, L., Lott, F., Ghattas, J., Braconnot, P., Marti, O., Meurdesoif, Y., and Bopp, L.: Climate and sensitivity of the IPSL-CM5A coupled model: impact of the LMDZ atmospheric grid configuration, submitted, Clim. Dynam., 2012. 518

Jost, A., Lunt, D., Kageyama, M., Abe-Ouchi, A., Peyron, O., Valdes, P., and Ramstein, G.: High-resolution simulations of the last glacial maximum climate over Europe: a solution to discrepancies with continental palaeoclimatic reconstructions?, Clim. Dynam., 24, 577–590, 2005. 524

Jost, A., Fauquette, S., Kageyama, M., Krinner, G., Ramstein, G., Suc, J.-P., and Violette, S.: High resolution climate and vegetation simulations of the Late Pliocene, a model-data comparison over western Europe and the Mediterranean region, Clim. Past, 5, 585–606, doi:10.5194/cp-5-585-2009, 2009. 518

Kamae, Y., Ueda, H., and Kitoh., A.: Hadley and Walker circulations in the mid-Pliocene warm period simulated by an atmospheric general circulation model, J. Meteor. Soc. Japan, 89, 475–493, 2011. 524, 526

Kasahara, A.: Computational aspects of numerical models for weather prediction and climate simulation, in: Methods in computational physics, edited by: Chang, J., Academic, Amsterdam, vol. 17, 1–66, 1977. 518

Koenig, S. J., DeConto, R. M., and Pollard, D.: Pliocene Model Intercomparison Project Experiment 1: implementation strategy and mid-Pliocene global climatology using GENESIS v3.0 GCM, Geosci. Model Dev., 5, 73–85, doi:10.5194/gmd-5-73-2012, 2012. 523, 524, 526

Krinner, G., Viovy, N., de Noblet-Ducoudre, N., Ogee, J., Polcher, J., Friedlingstein, F., Ciais, P., Sitch, S., and Prentice, I. C.: A dynamic global vegetation model for studies of the coupled atmosphere-biosphere system, Global Biogeochem. Cy., 19, GB1015, doi:10.1029/2003GB002199, 2005. 518, 519

Le Sommer, J., Penduff, T., Theetten, S., Madec, G., and Barnier, B.: How momentum advection schemes influence current-topography interactions at eddy permitting resolution, Ocean Model., 29, 1–14, doi:10.1016/j.ocemod.2008.11.007, 2009. 519

Leduc G., Schneider, R., Kim, J.-H., and Lohmann., G.: Holocene and Eemian sea surface temperature trends as revealed by alkenone and Mg/Ca paleothermometry, Quat. Sci. Rev., 29, 989–1004, 2010. 525

Lévy, M., Estublier, A. and Madec, G.: Choice of an advection scheme for biogeochemical models, Geophys. Res. Lett., 28, 3725–3728, doi:10.1029/2001GL012947, 2001. 519

Lott, F.: Alleviation of Stationary Biases in a GCM through a Mountain Drag Parameterization Scheme and a Simple Representation of Mountain Lift Forces, Mon. Weather Rev., 127, 788–801, 1999. 518

Lott, F., Fairhead, L., Hourdin, F., and Levan, P.: The stratospheric version of LMDz: dynamical climatologies, arctic oscillation, and impact on the surface climate, Clim. Dynam., 25, 851–868, 2005. 518

Madec, G.: NEMO ocean engine. Technical note, IPSL, available at: http://www.nemo-ocean.eu/content/download/15482/73217/file/NEMO_book_v3_3.pdf (last access: 17 February 2012), 2008. 519

Madec, G. and Imbard, M.-A.: Global ocean mesh to overcome the North Pole singularity, Clim. Dynam., 12, 381–388, 1996. 519

Madec, G., Delecluse, P., Imbard, M., and Levy C.: OPA version 8.1 Ocean general circulation model reference manual, 3. LODYC, Technical Report, 91 pp. available at: http://www.nemo-ocean.eu/About-NEMO/Reference-manuals, 1997. 519

Marti O., Braconnot, P., Dufresne, J.-L., Bellier, J., Benshila, R., Bony, S., Brockmann, P., Cadule, P., Caubel, A., Codron, F., de Noblet, N., Denvil, S., Fairhead, L., Fichefet, T., Foujols, M.-A., Friedlingstein, P., Goosse, H., Grandpeix, J.-Y., Guilyardi, E., Hourdin, F., Krinner, G., Lévy, C., Madec, G., Mignot, J., Musat, I., Swingedouw, D., and Talandier, C.: Key features of the IPSL ocean atmosphere model and its sensitivity to atmospheric resolution, Clim. Dynam., 34, 1–26, doi:10.1007/s00382-009-0640-6, 2010. 517, 518, 519, 520

Morcrette, J.: Radiation and cloud radiative properties in the European Centre for Medium Range Weather Forecasts forecasting system, J. Geophys. Res., 96, 9121–9132, 1991. 518

Murray, R. J.: Explicit generation of orthogonal grids for ocean models, J. Comput. Phys., 126, 251–273, 1996. 519

Ramstein, G., Serafini-Le Treut, Y., Le Treut, H., Forichon, M., and Joussaume, S.: Cloud processes associated with past and future climate changes, Clim. Dynam., 14, 233–247,

1998. 524

Ravelo, A. C., Andreasen, D. H., Lyle, M., Lyle, A. O., and Wara, M. W.: Regional climate shifts caused by gradual global cooling in the Pliocene epoch, Nature, 429, 263–267, 2004. 524, 525

Reynolds, R. W. and Smith, T. M.: A high resolution global sea surface temperature climatology, J. Climate, 8, 1571–1583, 1995. 521

Robinson, M. M., Dowsett, H. J., Dwyer, G. S., and Lawrence, K. T.: Reevaluation of mid-Pliocene North Atlantic sea surface temperatures, Paleoceanography, 23, PA3213, doi:10.1029/2008PA001608, 2008. 521, 524

Sadourny, R. and Laval, K.: January and July performance of the LMD general circulation model, in: New perspectives in climate modeling, edited by: Berger, A. and Nicolis, C., Elsevier, Amsterdam, 173–197, 1984. 518

Salzmann, U., Haywood, A. M., Lunt, D. J., Valdes, P. J., and Hill, D. J.: A new global biome reconstruction and data-model comparison for the Middle Pliocene, Global Eco. Biogeogr., 17, 432–447, 2008. 519, 521, 522

Salzmann, U., Haywood, A. M., and Lunt, D. J.: The past is a guide to the future?, Comparing Middle Pliocene vegetation with predicted biome distributions for the twenty-first century, Phil. Trans. R. Soc. A, 367, 189–204, 2009. 517

Sitch, S., Smith, B., Prentice, C., Arneth, A., Bondeau, A., Cramer, W., Kaplan, J. O., Levis, S., Lucht, W., Sykes, M. T., and Thonicke, K.: Evaluation of ecosystem dynamics, plant geography and terrestrial carbon cycling in the LPJ dynamic vegetation model, Glob. Change Biol., 9, 161–185, 2003. 518

Sloan, L. C., Crowley, T. J., and Pollard, D.: Modeling of middle Pliocene climate with the NCAR GENESIS general circulation model, Mar. Micropaleontol., 27, 51–61, 1996. 517

Sohl, L. E., Chandler, M. A., Schmunk, R. B., Mankoff, K., Jonas, J. A., Foley, K. M., and Dowsett, H. J.: PRISM3/GISS topographic reconstruction: US Geol. Surv. Data Series, 419, 6 pp., 2009. 521

Yan, Q., Zhang, Z., Wang, H., Gao, Y., and Zheng, W.: Set-up and preliminary results of mid-Pliocene climate simulations with CAM3.1, Geosci. Model Dev. Discuss., 4, 3339–3361, doi:10.5194/gmdd-4-3339-2011, 2011. 524, 526

Zhang, Z. S., Nisancioglu, K., Bentsen, M., Tjiputra, J., Bethke, I., Yan, Q., Risebrobakken, B., Andersson, C., and Jansen, E.: Pre-industrial and mid-Pliocene simulations with NorESM-L, Geosci. Model Dev. Discuss., 5, 119–148, doi:10.5194/gmdd-5-119-2012, 2012. 525, 527

Table 1. Conversion of biomes from PRISM3D to ORCHIDEE's Plant Functional Types. For the presence of one biome on a grid cell, is attributed a fractional value of one or several PFTs. The sum of the 13 PFT fractions (Fr) on each grid cell must be equal to 1. PFT1 = barren soil/desert. PFT2 = TrBE : Tropical Broadleaf Evergreen trees. PFT3 = TrBR: Tropical Broadleaf Raingreen trees. PFT4 = TeNE: Temperate Needleleaf Evergreen trees. PFT5 = TeBE: Temperate Broadleaf Evergreen trees. PFT6 = TeBS: Temperate Broadleaf Summergreen trees. PFT7 = BoNE: Boreal Needleleaf Evergreen trees. PFT8 = BoBS: Boreal Broadleaf Summergreen trees. PFT9 = BoNS: Boreal Needleleaf Summergreen trees. PFT10 = NC3: Natural C3 grass. PFT11 = NC4: Natural C4 grass.

BIOME	Fr	PFT	BIOME	Fr	PFT
1 Tropical evergreen forest	1	2 TrBE	2 Tropical semi_deciduous forest	0.5 0.5	2 TrBE 3 TrBR
3 Tropical deciduous forest/woodland	0.7 0.3	3 TrBR 11 NC4	4 Temperate deciduous forest	0.1 0.1 0.8	4 TeNE 5 TeBE 6 TeBS
5 Temperate conifer forest	0.8 0.1 0.1	4 TeNE 5 TeBE 6 TeBS	6 Warm-temperate mixed forest	0.1 0.4 0.5	4 TeNE 5 TeBE 6 TeBS
7 Cool mixed forest	0.4 0.4 0.1 0.1	4 TeNE 6 TeBS 7 BoNE 8 BoBS	8 Cool conifer forest	0.8 0.2	4 TeNE 6 TeBS
9 Cold mixed forest	0.4 0.5 0.1	7 BoNE 8 BoBS 9 BoNS	10 Evergreen taiga/ montane forest	0.9 0.1	7 BoNE 8 BoBS
11 Deciduous taiga/ montane forest	0.3 0.7	8 BoBS 9 BoNS	12 Tropical savanna	0.3 0.2 0.5	3 TrBR 10 NC3 11 NC4
13 Tropical xerophytic shrubland	0.2 0.3 0.5	1 Barren 3 TrBR 11 NC4	14 Temperate xerophytic shrubland	0.2 0.2 0.6	1 Barren 5 TeBE 10 NC3

Table 1. Continued.

BIOME	Fr	PFT	BIOME	Fr	PFT
15 Temperate sclerophyll woodland	0.3 0.3 0.4	4 TeNE 5 TeBE 10 NC3	16 Temperate broadleaved savanna	0.2 0.2 0.6	5 TeBE 6 TeBS 10 NC3
17 Open conifer woodland	0.4 0.6	4 TeNE 10 NC3	18 Boreal parkland	0.1 0.2 0.1 0.6	7 BoNE 8 BoBS 9 BoNS 10 NC3
19 Tropical grassland	0.1 0.03 0.87	1 Barren 3 TrBR 11 NC4	20 Temperate grassland	0.03 0.97	5 TeBE 10 NC3
21 Desert	1	1 Barren	22 Steppe tundra	0.3 0.7	1 Barren 10 NC3
23 Shrub tundra	0.3 0.7	8 BoBS 10 NC3	24 Dwarf-shrub tundra	0.2 0.8	8 BoBS 10 NC3
25 Prostrate shrub tundra	0.1 0.9	8 BoBS 10 NC3	26 Cushion-forb lichen moss tundra	0.1 0.9	1 Barren 10 NC3
27 Barren soil	1	1 Barren	28 Land ice	1	1 Barren

Table 2. Comparative table of global mean values for the AGCM and AOGCM mid-Pliocene simulations.

Variable	Units	AGCM absolute	AGCM anomaly to Ctrl	AOGCM absolute	AOGCM anomaly to Ctrl
Surface air temperature	˚C	17	1.94	14.9	1.83
Total precipitation	$\mathrm{mm\,day^{-1}}$	2.89	0.05	2.77	0.11
Rainfall	$\mathrm{mm\,day^{-1}}$	2.75	0.09	2.59	0.13
Snowfall	$\mathrm{mm\,day^{-1}}$	0.14	−0.04	0.18	−0.02
Sea surface temperature	˚C	19.75	1.5	17.88	1.25
Sea surface salinity	psu	–	–	34.34	−0.09
TOA net down radiative flux	$\mathrm{W\,m^{-2}}$	2.43	3.66	0.81	0.80

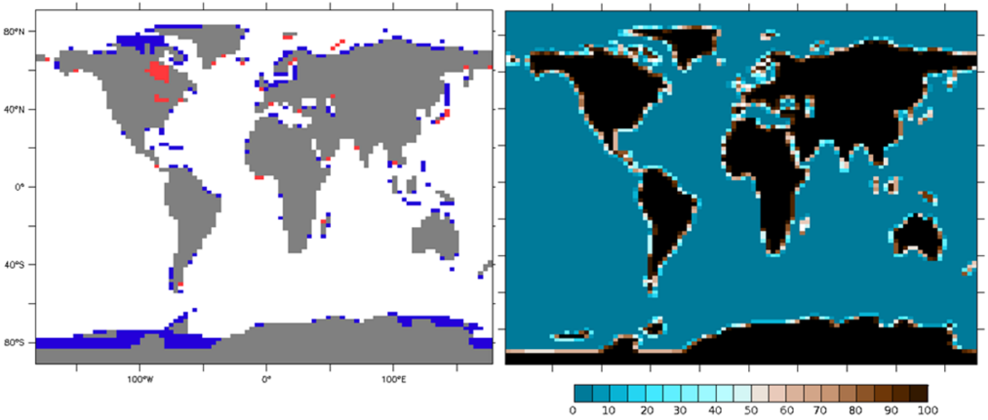

Fig. 1. Left: difference between present land-sea mask and mPWP land-sea mask. Blue grid cells are land in the present mask (i.e. land fraction superior or equal to 50 %), but ocean in the mPWP mask. Red grid cells are ocean in the present mask and land in the mPWP mask. Right: land percentage on each grid cell for the "preferred" simulation.

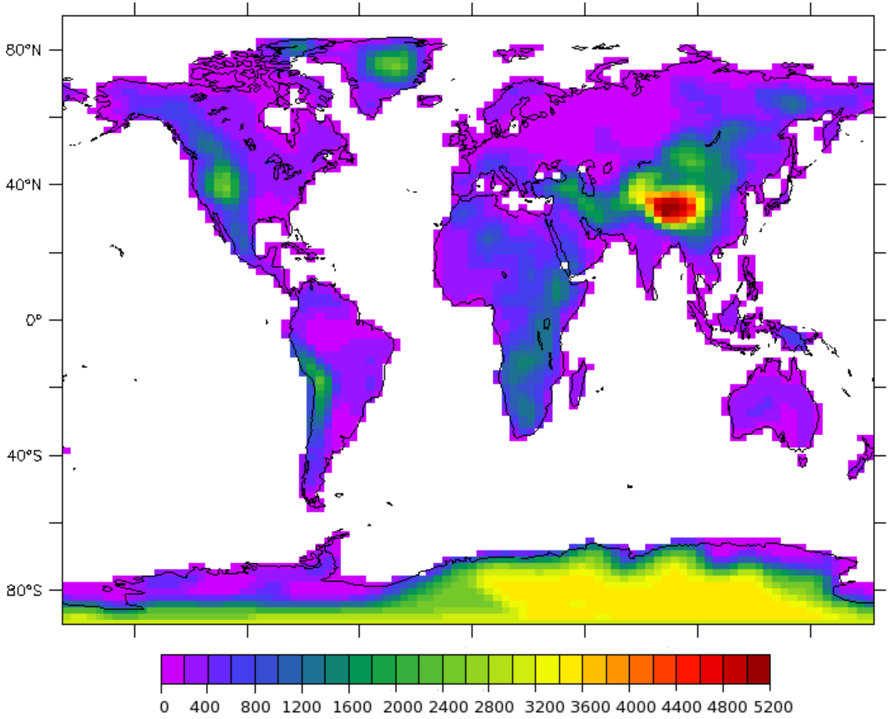

Fig. 2. Absolute implemented mid-Pliocene topography calculated via the anomaly method, expressed in meters.

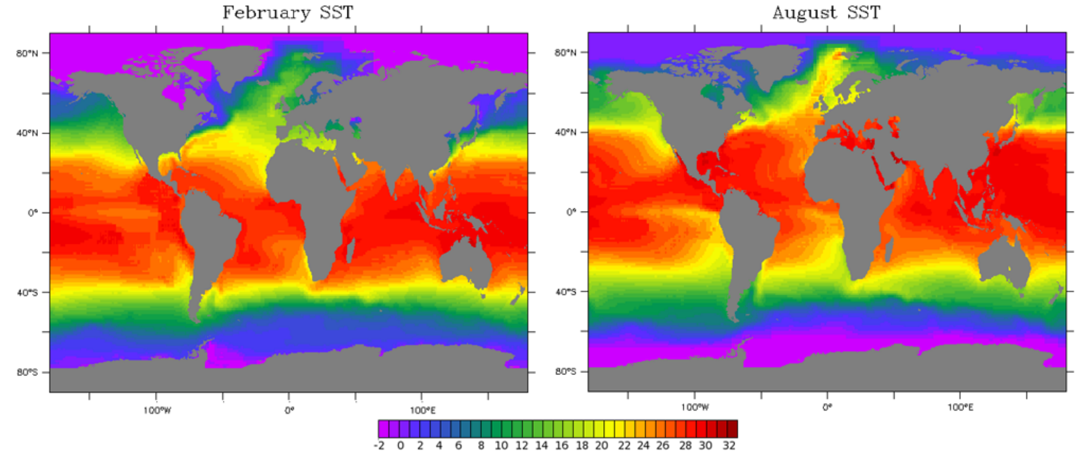

Fig. 3. Mid Pliocene sea surface temperatures imposed for February (left) and August (right), expressed in degrees Celsius.

Title Page
Abstract Introduction
Conclusions References
Tables Figures
◀| |▶
◀ ▶
Back Close
Full Screen / Esc
Printer-friendly Version
Interactive Discussion

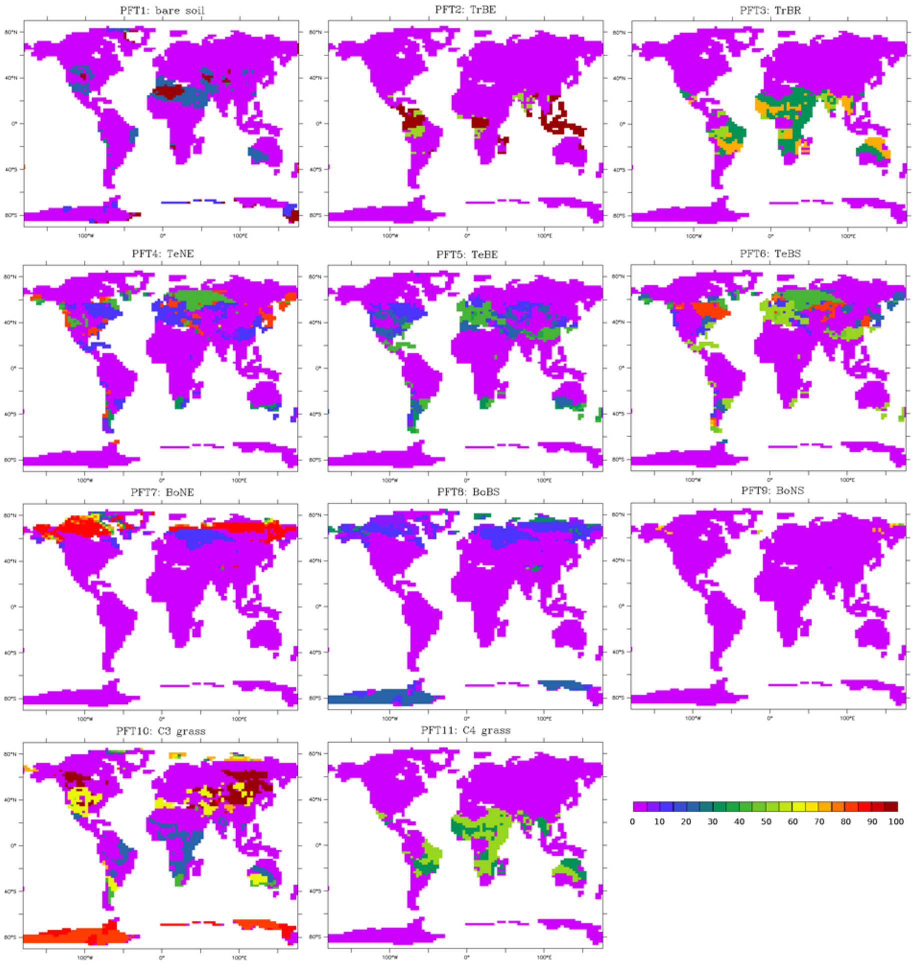

Fig. 4. mPWP imposed percentage of each PFT in the ORCHIDEE model, on the "alternate" land-sea mask for every grid cell where land fraction is superior to zero.

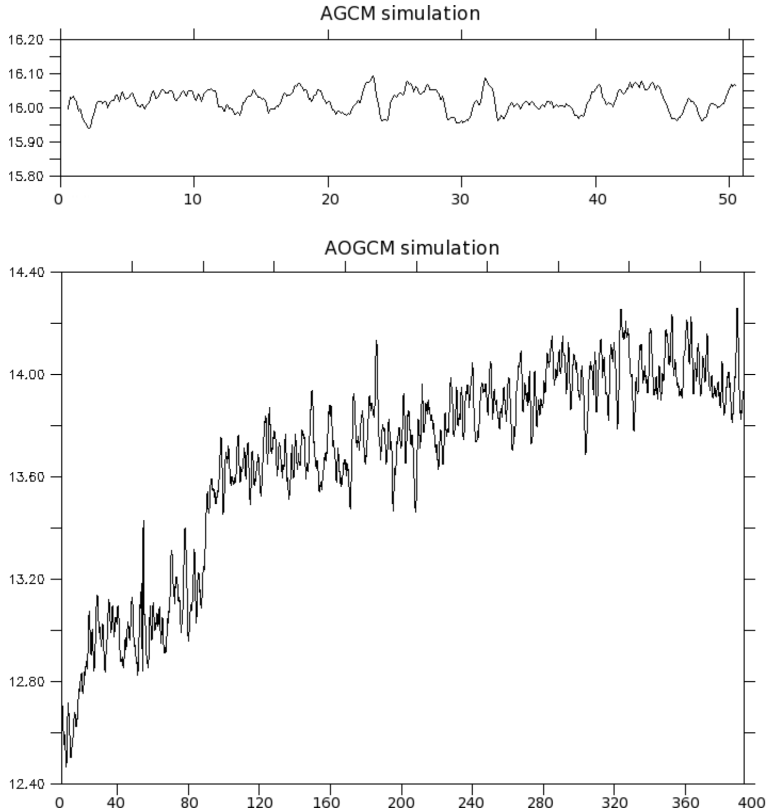

Fig. 5. Evolution of the globally averaged 2 m temperature for the AGCM and AOGCM, expressed in degrees Celsius.

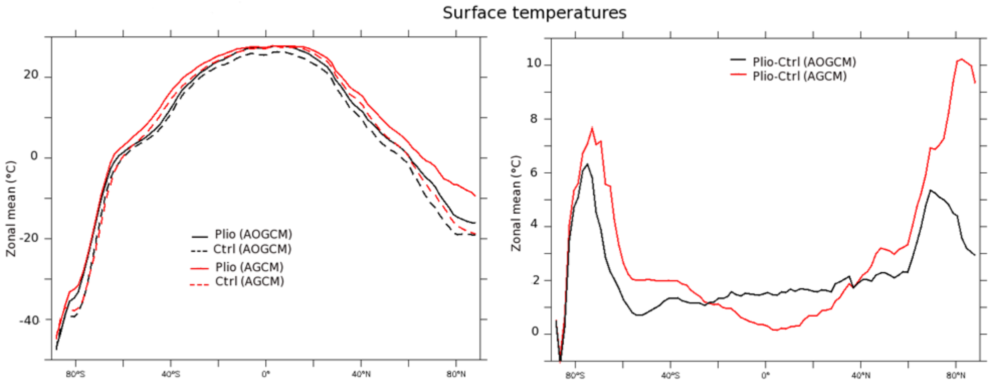

Fig. 6. Zonal mean surface temperature for the mid-Pliocene experiments and the control (left), and zonal mean surface temperature anomaly to the control for both Pliocene experiments (right), expressed in degrees Celsius.

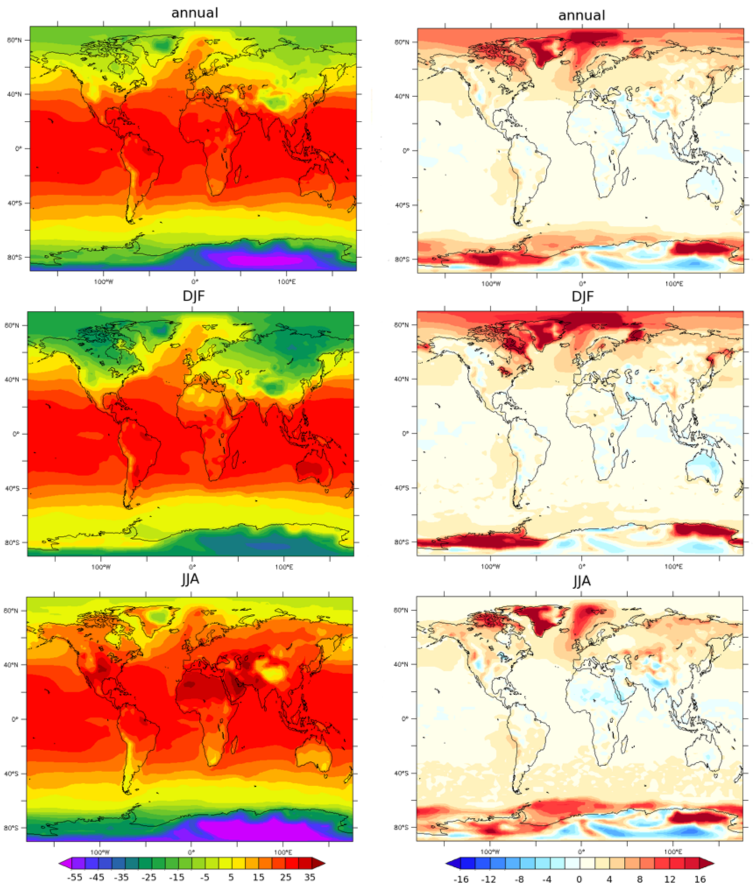

Fig. 7. AGCM mid-Pliocene (Plio1_alt) mean surface temperatures (left) for yearly average, December-January-February, June-July-August, and their anomaly to the control (right), expressed in degrees Celsius.

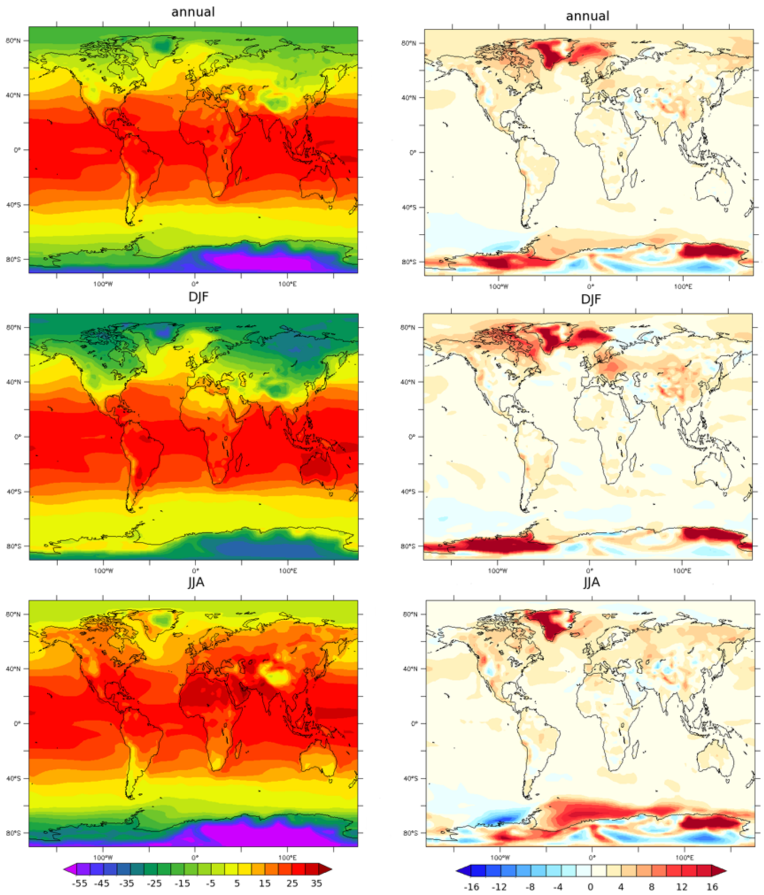

Fig. 8. AOGCM mid-Pliocene mean surface temperatures (left) for yearly average, December-January-February, June-July-August, and their anomaly to the control (right), expressed in degrees Celsius.

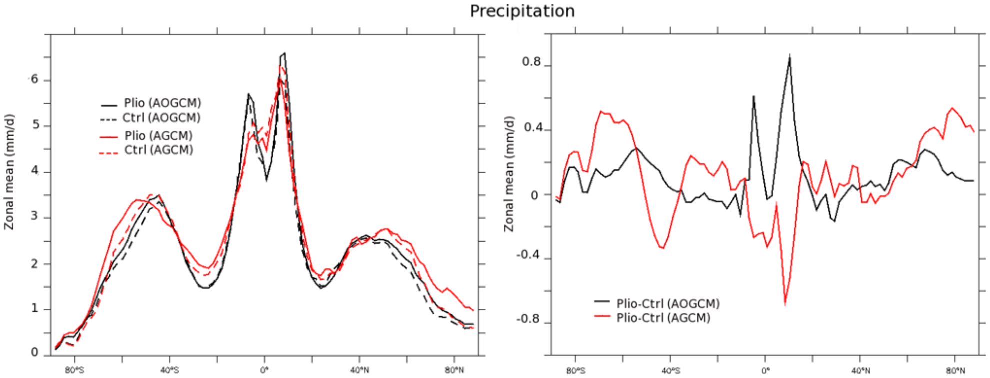

Fig. 9. Zonal annual mean precipitation for the control and the mid-Pliocene experiments (left). Zonal mean precipitation anomaly to the control for both Pliocene experiments (right).

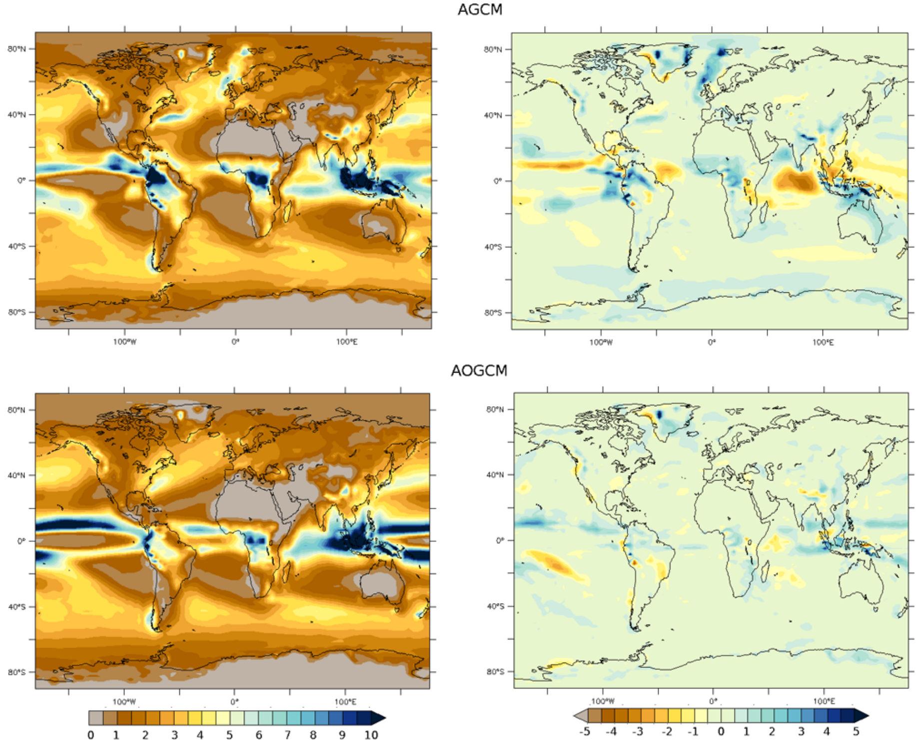

Fig. 10. Mid-Pliocene mean annual precipitation (left) for AGCM (top) and AOGCM (bottom), and their anomaly to the control (right), expressed in mm day^{-1}.

Title Page
Abstract
Introduction
Conclusions
References
Tables
Figures
◀I
▶I
◀
▶
Back
Close
Full Screen / Esc
Printer-friendly Version
Interactive Discussion

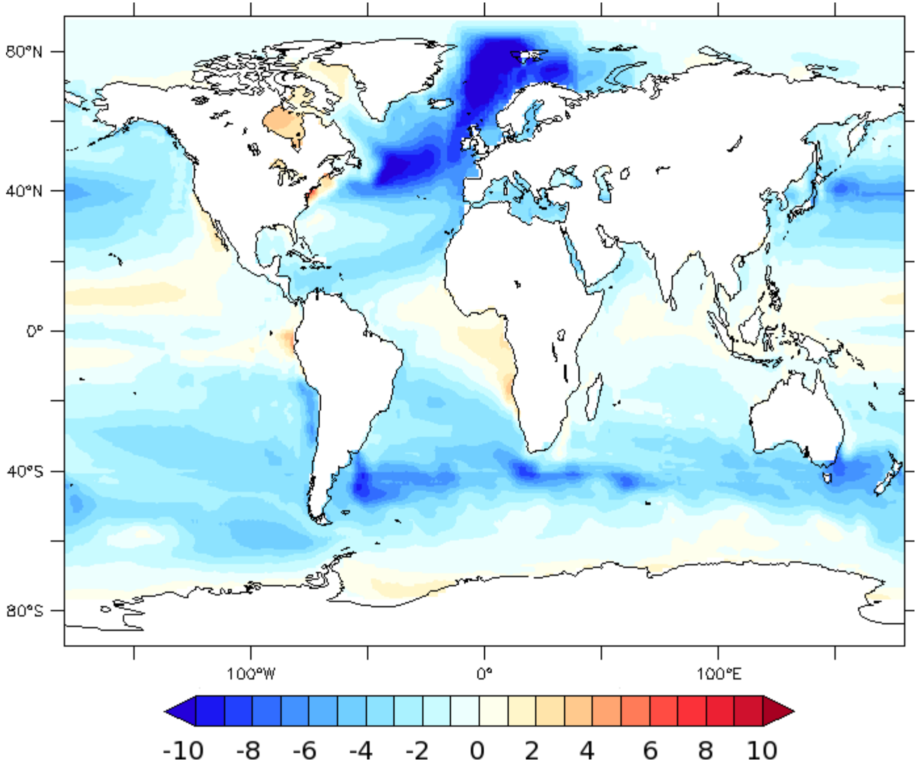

Fig. 11. Difference between AOGCM simulated mid-Pliocene SSTs and AGCM mid-Pliocene imposed SSTs.

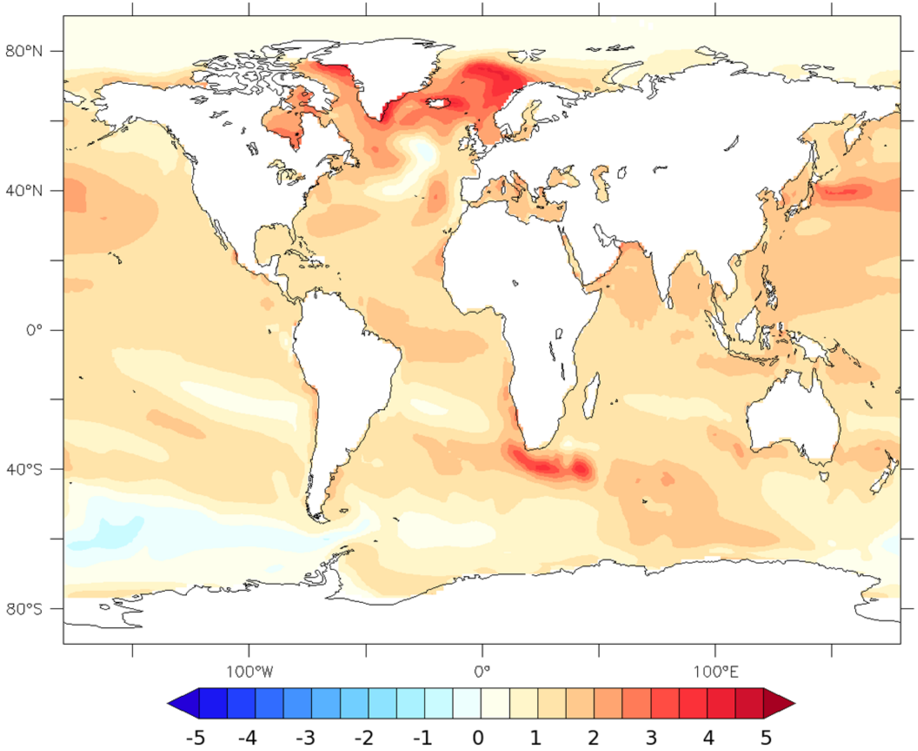

Fig. 12. Difference between AOGCM simulated mid-Pliocene SSTs and AOGCM simulated Pre-industrial SSTs.

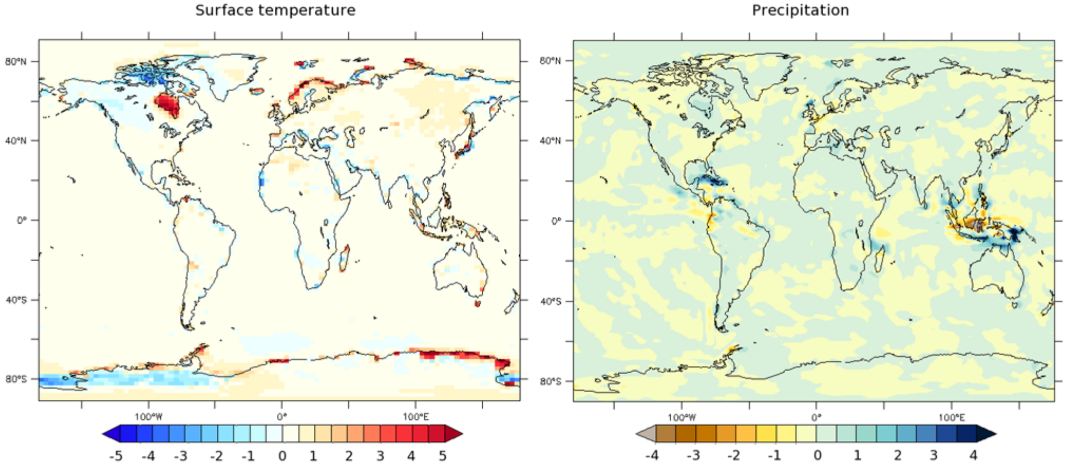
Surface temperature

Precipitation

Fig. 13. Surface temperature difference between the "preferred" AGCM simulation and the "alternate" AGCM simulation, i.e. Plio1_pref minus Plio1_alt, expressed in degrees Celsius (left) and total precipitation difference (Plio1_pref minus Plio1_alt) expressed in mm day^{-1} (right).